Carbon-modified Bi_2WO_6 nanostructures with improved photocatalytic activity under visible light

Yuanyuan Li,*[a] Jinping Liu,[b] Xintang Huang[b] and Jiaguo Yu*[a]

Received 23rd November 2009, Accepted 4th February 2010
First published as an Advance Article on the web 2nd March 2010
DOI: 10.1039/b924584g

Carbon-modified Bi_2WO_6 (C–Bi_2WO_6) nanostructures were synthesized *via* a hydrothermal process in the presence of glucose followed by the calcination in Ar gas at 500 °C. The morphologies and crystallinity of Bi_2WO_6 and the nature of carbon in the composites obtained with different glucose amounts were characterized. Raman spectrum analysis, electron microscopy results and light absorption of C–Bi_2WO_6 at wavelengths larger than 450 nm clearly confirmed the carbon modification. Further results indicated that glucose did not affect the final crystalline structure or the band gap of Bi_2WO_6, but it had great influences on the photocatalytic activity of Bi_2WO_6 towards rhodamine-B (RhB) degradation. When the glucose amount was less than 0.04 g, the photoactivity was enhanced step by step with an increase in the glucose amount. The improved photocatalytic performance could be ascribed to the enhanced photogenerated electron-hole separation and more RhB adsorption associated with carbon. However, when the glucose amount was higher than 0.04 g, the photocatalytic property dramatically decreased due to the severe absorption of almost incident light by carbon, which hindered the accessibility of light to Bi_2WO_6. Our work provides an alternative way to improve the photoactivity of Bi_2WO_6 nanomaterials.

1 Introduction

On the basis of the general accepted objective to achieve efficient utilization of visible light solar radiation to address the global environmental and energy problems, many efforts have been made to develop other heterogeneous visible light-driven photocatalysts besides those resulting from the modification of TiO_2 for their application in degrading harmful molecules and generating H_2 from water. To date, a large number of reports have demonstrated that many complex ternary metal oxides[1-10] have visible light-induced photocatalytic activity, while doping TiO_2 with transition-metal cations[11-13] or non-metal anions[14-18] (such as N, S, C, F), depositing some noble metal nanoparticles[19-21] on and coupling narrow-band metal oxides[22,23] with TiO_2 can successfully extend photocatalytic activity of TiO_2 into the visible range.

It is widely accepted that an efficient photocatalytic process should possess[24] (1) a high mobility for photoexcited electron-hole separation, (2) a fair visible light responsive ability to maximally utilize the sunlight energy, (3) suitable band potentials for the oxidation of organic molecules and (4) high absorption of organic contaminant for photocatalytic destruction. Among these requirements, the first one is especially important and has significant benefits for the improvement of the catalytic performance of photocatalysts.[25] There are several approaches to accelerate the charge carrier separation. For example, noble metal decoration[26,27] can enhance the efficiency of the interfacial charge transfer process through the formation of a "Schottky" barrier between the metal and the semiconducting photocatalyst, which can be attributed to the different Fermi levels of the metal and the semiconductors. An alternative method is a semiconductor coating[28,29] that can improve the charge separation in the photocarrier generation process through the synergetic effect between the coupled semiconductors and photocatalysts caused by their suitable band levels. Also, there were several recent publications that reported a novel method, that is carbon modification,[30-37] to accelerate the charge transfer from photocatalyst to the liquid–solid interface contacted with organic pollutants by taking advantage of carbon's unique electron transport properties, which is completely different from the carbon doping mechanism in previous studies. However, these studies mostly focused on TiO_2 and ZnO nanostructures.

Bi_2WO_6, which has a layered structure with perovskite-like slabs of WO_6 and $[Bi_2O_2]^{2+}$ layers, has been shown to be a promising visible light-driven photocatalyst[38,39] for its activity of O_2 evolution and dye decomposition. By a typical hydrothermal process, a wide spectrum of Bi_2WO_6 micro-/nanostructures including nanoparticles,[40,41] nanoplates,[42-44] and complex superstructures (solid and hollow spheres, octahedron, *etc.*)[45-48] were synthesized. Among these, various complex structures were proposed to have advantages of efficient visible light transmission and utilization, enhanced dye absorption and good recyclability. High surface-to-volume nanoplates were designed for fast separation/transfer of photoexcited electrons and holes. On the other hand, in order to further improve the separation of photogenerated electron-hole pairs and finally optimize the photocatalytic activity, few reports show the construction of coupled semiconductor nanojunction systems such as Co_3O_4–Bi_2WO_6,[49] C_{60}–Bi_2WO_6[50] and AgBr–Ag–Bi_2WO_6.[51] However, these composite photocatalysts either contain

[a]*State Key Laboratory of Advanced Technology for Materials Synthesis and Processing, Wuhan University of Technology, Wuhan, 430070, P. R. China. E-mail: liyynano@yahoo.com.cn, jiaguoyu@yahoo.com*
[b]*Department of Physics, Central China Normal University, Wuhan, 430079, P. R. China*

toxic ions (Co^{3+}) or are expensive (C_{60}, Ag); how to design environmentally benign, inexpensive and highly-efficient Bi_2WO_6-based photocatalysts remains a huge challenge.

Herein, we present the synthesis of a carbon-modified Bi_2WO_6 (C–Bi_2WO_6) nanostructured photocatalyst through a simple combination of hydrothermal and post-calcination processes. The effect of carbon on the photocatalytic activity of Bi_2WO_6 has been investigated in detail. It is found that the presence of an appropriate amount of carbon could significantly improve the photodegradation property of Bi_2WO_6 towards rhodamine-B (RhB).

2 Experimental

2.1 Synthesis of C–Bi_2WO_6 samples

All chemical reagents in this study were of analytical grade and used without further purification.

In our work, a C–Bi_2WO_6 nanostructure was synthesized by a two-step process. The first step was carried out to fabricate the precursor of C–Bi_2WO_6 by a hydrothermal method in aqueous solution containing glucose at 180 °C for 12 h. In a typical example, Na_2WO_6 (1 mmol), $Bi(NO_3)_3$ (2 mmol) and a certain amount of glucose were added successively into 80 mL distilled water with strong stirring followed by 10 min ultrasonication. Plenty of white precipitation appeared after the addition, which was then transferred into a Teflon-lined stainless steel autoclave (V = 100 mL). The autoclave was sealed and maintained at 180 °C for 12 h. After the reaction, the product was collected *via* centrifugation and dried in an oven at 60 °C. The second step was calcination: C–Bi_2WO_6 nanostructure was achieved by calcining the hydrothermal product at 500 °C for 3 h in Ar flow in a tube furnace. Products prepared with different amounts of glucose (0.005 g, 0.02 g, 0.04 g, 0.2 g) after the hydrothermal process were named as H180-1, H180-2, H180-3, H180-4, while those obtained after calcination were denoted as C500-1, C500-2, C500-3 and C500-4, respectively. Experimental details and more information on the products are listed in Table 1.

For a comparative study, pristine Bi_2WO_6 powder was also synthesized without the use of glucose during the hydrothermal process. It was named as H180-0 and its calcined product under the same annealing conditions described above was denoted as C500-0.

2.2 Characterizations

The morphologies of the as-prepared products were characterized by field-emission scanning electron microscopy (FESEM, JEOL, JSM-6700F) operated at an acceleration voltage of 5.0 kV. The crystalline structures of the products were analyzed by an X-ray diffractometer (XRD, Y-2000) with Cu Kα radiation (λ = 1.5418 Å) at a scanning rate of 0.04° s^{-1}. Transmission electron microscopy (TEM and HRTEM) observations were carried out on a JEOL JEM-2010 instrument in a bright field, and selected area electron diffraction (SAED) modes were carried out on a HRTEM JEM-2010FEF instrument (operated at 200 kV). Room-temperature -vis absorption spectra were recorded on a Lambda35 spectrophotometer in the wavelength range of 200–900 nm. The nitrogen adsorption–desorption isotherm and Barrett–Joyner–Halenda (BJH) methods were analyzed on a Bel Sorp-mini (S/N-00230) Analyzer (accelerated surface area and porosimetry system). Raman spectra were acquired with a Raman microspectrometer (Renishaw 1000 NR) using an Argon ion laser (632.8 nm). Raman spectra were measured using a microscope equipped with a 20× objective which focused the incident excitation laser radiation into a spot 1–2 mm or 2–3 mm in diameter, respectively, and the scattered light was collected.

2.3 Photocatalytic activity test

Photocatalytic activity was evaluated by the degradation of RhB under visible light irradiation using a 300 W halogen-tungsten lamp with a cutoff filter (λ > 400 nm). The reaction cell was placed in a sealed black box, of which the top was open and the cutoff filter was set on the window face of the reaction cell to ensure the desired irradiation condition. In each experiment, photocatalyst powders (2 g L^{-1}) were added into RhB solution (1×10^{-5} M, 100 mL). Before illumination, the suspensions were magnetically stirred in the dark for 60 min to ensure the establishment of an adsorption–desorption equilibrium between the photocatalyst powders and RhB. At given time intervals, 3 mL aliquots were sampled and centrifuged to remove photocatalyst powders. The filtrates were analyzed by recording the variations of the absorption-band maximum (553 nm) of RhB in the UV-vis spectrum.

3 Results and discussion

After the hydrothermal process (H180 series), the color of all samples was light yellow, as observed from the naked eye. Fig. 1a shows the X-ray diffraction patterns of all H180 samples synthesized with different amounts of glucose. The results illustrate that all H180 samples are pure Bi_2WO_6. No other diffraction peaks can be observed, demonstrating that glucose used in the hydrothermal synthesis does not have an effect on the crystalline phase of Bi_2WO_6. Generally speaking, the hydrothermal carbonization degree of glucose in our case is very low, leading to the formation of a small quantity of carbonaceous species; that's the reason why the color of the products changes little even with the glucose

Table 1 Experimental details about the synthesis of C–Bi_2WO_6 samples

No.	Mass of glucose/g	Sample names after hydrothermal process	Colors of H180 samples	Sample names after calcination process	Colors of C500 samples
1	0	H180-0	Light yellow	C500-0	Light yellow
2	0.005	H180-1	Light yellow	C500-1	Light grey
3	0.02	H180-2	Light yellow	C500-2	Grey
4	0.04	H180-3	Light yellow	C500-3	Grey
5	0.2	H180-4	Light yellow	C500-4	Brown-grey

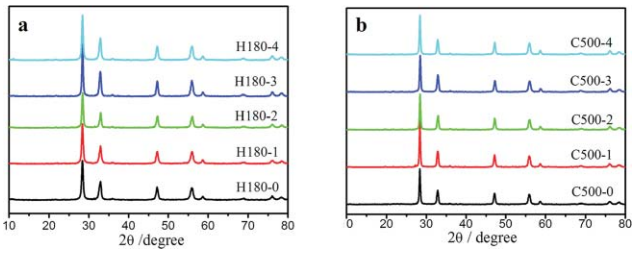

Fig. 1 XRD patterns of H180 and C500 samples.

addition. Similar XRD patterns are further obtained from C500 samples (Fig. 1b), with a slight increase of peak intensity compared to uncalcined samples. The colors of the calcined products have changed, as given in Table 1. The calcined sample with 0.005 g glucose during the hydrothermal process is light grey, and that obtained using 0.2 g glucose is brown-grey, indicating that the carbon content increases in the C500 samples with an increase in the amount of glucose. Although the transformation of products' color from light yellow to light grey and finally to brown-grey can be clearly observed, the XRD peaks from carbon could not be obviously observed for all C500 samples. This can be attributed to the small mass of glucose used during the synthesis and the relatively low graphitization degree of carbon.

The morphologies of all products were examined by SEM. Sample H180-0 obtained in the absence of glucose represents a loose two-dimensional (2D) plate-like structure consisting of primary square nanoplates, as shown in Fig. 2a. This growth habit is associated with the crystal structure of Bi_2WO_6 and consistent with those reported previously.[42,47] After calcination (sample C500-0), the subunit nanoplates shrink into larger ellipsoidal particles, while the overall shape of the structure has little change. In the presence of glucose, the morphology of the product changes after the hydrothermal process. It was reported that glucose could be transformed into various carbonaceous species under hydrothermal conditions,[42-54] which may act as "surfactant", absorbing on the surface of Bi_2WO_6 grains and affecting the crystal growth. As can be seen, with the use of 0.005 g or 0.02 g glucose, some three-dimensional (3D) hierarchical structures emerge except for 2D plates (Fig. 2c), and they can keep the morphology unchanged after calcination (Fig. 2d). However, when the amount of glucose increases to 0.04 g or 0.2 g, little aggregated nanoplates are dominant in the products (Fig. 2e); they become larger dispersed nanoparticles after calcination (Fig. 2f). From Fig. 2b, 2d and 2f, we can also observe that all calcined samples (C500) consist of subunit nanoparticles with similar shape and size. It is worthy to point out that no byproducts such as carbon spheres can be found in the H180 samples, further confirming that in our case the carbonization of glucose was not finished under hydrothermal conditions. The acidic starting solution may reduce the hydrothermal carbonization degree of glucose. As a result, the calcination process can be employed to achieve the carbon-decorated samples.

More structural information of the C–Bi_2WO_6 nanostructures was obtained from TEM observations. The HRTEM image taken on an individual C–Bi_2WO_6 nanoparticle (sample C500-3) exhibits a group of clear parallel crystal planes with the interspacing of 0.272 nm, corresponding to the (200) plane of orthorhombic Bi_2WO_6 (Fig. 3a and 3b). The fast Fourier transform (FFT) pattern in the inset further confirms the single crystal structure of Bi_2WO_6. A poorly-crystallized carbon layer with a thickness of 2 nm can also be observed (see arrows). On the surface of another C–Bi_2WO_6 particle (Fig. 3c), there are some obvious "dark dots" presented (amorphous overlayer on crystal lattice), as indicated by circles. The presence of these dots is most likely due to the carbon modification.

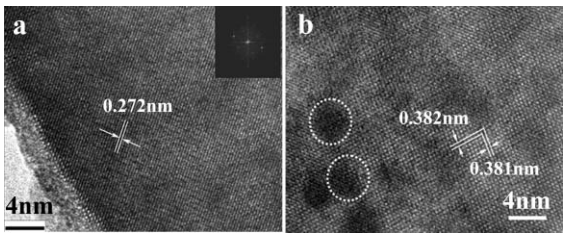

Fig. 3 The HRTEM images of C500-3 sample. Inset is the corresponding FFT pattern of Fig. 3a.

Fig. 4a shows Raman spectra of typical C500 samples (C500-0, C500-2, C500-3, and C500-4). C500-0, a pure calcined Bi_2WO_6, has several peaks in the range of 600–1000 cm^{-1}, which can be assigned to the stretches of the W–O bands.[55] In detail, the bands at 790 and 820 cm^{-1} are associated with antisymmetric and symmetric A_g modes of terminal O–W–O, respectively. The band at 310 cm^{-1} can be assigned to translational modes involving simultaneous motions of Bi^{3+} and WO_6^{6-}. The intensity of the peak at 700 cm^{-1} is interpreted as an antisymmetric bridging mode associated with the tungstate chain.[55] With the glucose content increasing, the intensity of inherent Raman peaks of Bi_2WO_6 decreases step by step. It should be pointed out that some peaks around 310 cm^{-1}

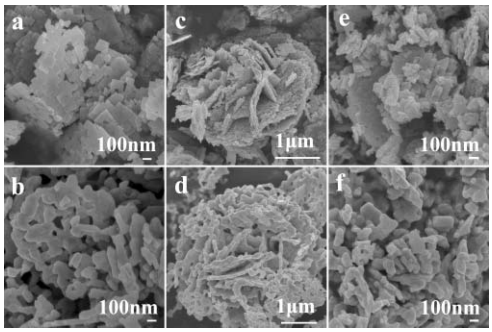

Fig. 2 SEM images of H180 and C500 samples: (a) H180-0, (b) C500-0, (c) H180-1, (d) C500-1, (e) H180-3 and (f) C500-3.

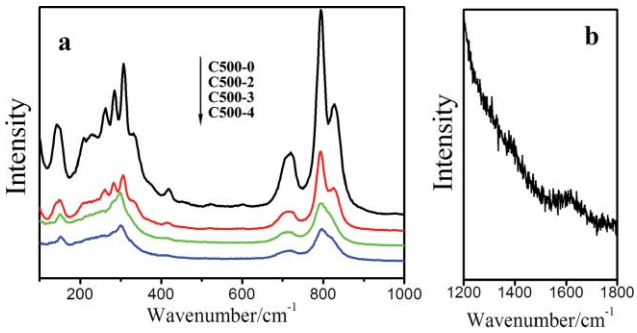

Fig. 4 Raman spectra of (a) C500-0, C500-2, C500-3, C500-4 and (b) C500-3 exhibiting graphitic modes.

and the peak at 820 cm^{-1} totally disappear when the amount of glucose achieves 0.2 g. Both the observations demonstrate that the existed carbon on the Bi_2WO_6 surface has a significant effect on the Raman property of Bi_2WO_6, indicating a strong interaction between Bi_2WO_6 and carbon (although carbon does not affect the crystal structure of Bi_2WO_6, as evidenced by XRD).

We also investigated the nature of the carbon present in the C500 samples by Raman spectroscopy at a longer wavelength range. Fig. 4b shows two weak peaks at 1380 and 1596 cm^{-1} for C500-3; the Raman spectra of other C500 samples in 1200–1800 cm^{-1} range show similar results. The peak at 1596 cm^{-1} (G-band) is considered as characteristic for E_{2g} mode of graphite, while 1380 cm^{-1} (D-band) is due to the presence of defect within the hexagonal graphitic structure.[33] The integrated intensity ratio of G- and D-band is usually used to character the degree of graphitization. The value is very low in the present work, indicating that carbon in C500 samples has a low degree of graphitization and much structural defects; this can be ascribed to the relatively low calcination temperature. Even under these conditions, the modified carbon still has a pronounced positive effect on the photocatalytic property of Bi_2WO_6, as will be discussed later.

The optical absorption of various C–Bi_2WO_6 samples (H180-0 and C500 series) was tested by UV-vis diffuse reflectance spectroscopy, and the results are shown in Fig. 5. After calcination, pure Bi_2WO_6 (C500-0) has an improved absorption in both UV and visible range of 450–800 nm, and the absorption edge has a little shift to long wavelength, which is due to the grain size increasing after calcination as observed in SEM results. With glucose in the hydrothermal process, all the C500 samples have a strongly broad background visible absorption at wavelength larger than 450 nm. In addition, the absorption increases with increasing the amount of glucose when it is not more than 0.04 g. The absorption edges of C500-1, C500-2, C500-3 and C500-4 samples are almost the same as that of the pure calcined Bi_2WO_6 (C500-0), indicating the identical band gap energy. This is contrary to the earlier C-doped TiO_2 nanomaterials that had a decrease in band gap energy of TiO_2. Combined with the aforementioned results, the carbon in the C500 samples should be free and decorated on the Bi_2WO_6 surface.

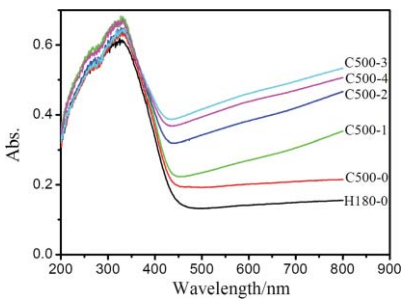

Fig. 5 UV-vis diffuse reflection spectra of H180-0, C500-0, C500-1, C500-2, C500-3 and C500-4 samples.

The photocatalytic activity of C500 samples was evaluated by degradation of RhB, a dye pollutant difficult to self-decompose. RhB is also a common model compound to test the photodegradation capability of photocatalysts. Fig. 6 shows the time profile of degradation ratio R_d% under visible light, where R_d% is defined by eqn (1). C_t is the concentration of RhB at the irradiation time t

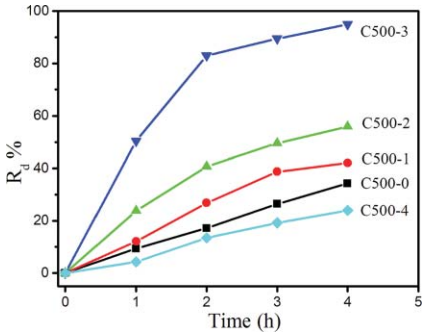

Fig. 6 The photodegradation curves of C500 samples under visible light irradiation.

and C is the concentration at the absorption equilibrium between the photocatalysts and dye before irradiation.

$$R_d\% = (C - C_t)/C \quad (1)$$

Among these samples, C500-1, C500-2, and C500-3 exhibit a gradually enhanced photoactivity for RhB degradation as compared to pure Bi_2WO_6, and C500-3 shows the highest photoactivity. After 4 h visible light irradiation, about 95% of RhB can be degraded in the presence of C500-3, but the R_d% is only about 34% with the use of C500-0. The temporal evolution of the absorption spectra of RhB was also carried out to investigate the concentration change of RhB during the photodegradation in the presence of C500-3, as shown in Fig. 7. The major absorption band of RhB is at 553 nm. The intensity of the major band has a sharp decrease after absorption equilibrium, indicating the strong absorption of the photocatalyst to the dye; the sufficient dye absorption can benefit the efficiency of photocatalysis. As the irradiation time increases, the major band decreases gradually and shifts to the short wavelength with the color of dye solution changing from initial red to light green-yellow, indicating that RhB is de-ethylated step by step.[48] Generally, as the amount of glucose during the hydrothermal process increases, the degradation efficiency of C–Bi_2WO_6 photocatalyst to RhB is enhanced. This can be explained by the fact that both the specific surface area (S_{BET}), and the adsorption efficiency to dye of C–Bi_2WO_6, increase with more glucose used, as seen in Table 2. The adsorption efficiency to dye (R_a%) is defined by eqn (2) where C_0 is the concentration of RhB before the absorption equilibrium. However, there is an optimal amount of glucose for photocatalysis. Once an excess amount of glucose is used, the photocatalytic activity will decrease drastically. In our work, the C500-4 sample, with 0.2 g glucose used during the hydrothermal process, displays very low photoactivity, even worse than pure calcined Bi_2WO_6 (C500-0) (Fig. 6).

$$R_a\% = (C_0 - C)/C_0 \quad (2)$$

Table 2 The surface areas (S_{BET}), adsorption efficiency (R_a%) and degradation efficiency (R_d%) of the C500 samples

	C500-0	C500-1	C500-2	C500-3	C500-4
$S_{BET}/m^2\ g^{-1}$	4.13	4.5	4.7	6.5	6.3
R_a%	8.1%	13.7%	22.5%	53.2%	50.5%
R_d%	34.3%	42.1%	55.7%	95.0%	24.0%

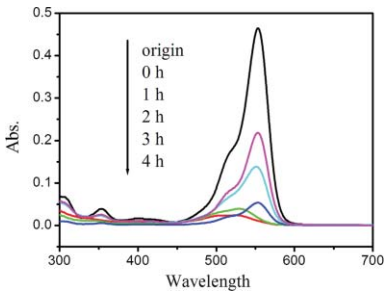

Fig. 7 The temporal evolution of the spectra during the photodegradation of RhB mediated by C500-3 sample under visible light irradiation. "Original" means the concentration before absorption equilibrium.

Under hydrothermal conditions, various chemical reactions of glucose can take place and result in the formation of complex organic compounds, which can absorb on the surface of Bi_2WO_6 grains and are further carbonized by calcination. There is a relationship between the amount of glucose and the color of calcined sample as discussed above. More importantly, the carbon existing in the C–Bi_2WO_6 nanostructures has effects on the BET surface area of the photocatalyst and the separation of photogenerated charges, *etc*; all of these parameters are strongly related to the photocatalytic performance of the photocatalyst. Based on the above experimental results, we have demonstrated that an optimized amount of glucose is essential to enhance the photoactivity. The C500-3 sample prepared by using 0.04 g glucose during the hydrothermal process exhibits the highest photocatalytic ability, which is due to the synergic effect of the obvious improvement in the nanostructure surface area and absorption of the dye, and the fast transfer rate of photogenerated electrons from Bi_2WO_6 to organic pollution through carbon (the photoexcited electrons further reduce O_2 into $O_2^{\bullet-}$ which can oxidize RhB[48]). Herein, we emphasize that carbon can significantly facilitate the separation of photogenerated electron-holes and improve the transportation of electrons, considering that carbon is a material with high conductivity.[33] This is the main reason why C–Bi_2WO_6 samples (C500-1, C500-2 and C500-3) have a much better performance than C500-0. However, the excess glucose during the hydrothermal period will lead to excessive carbon, thus make the photocatalyst fully coated with a thick and dense carbon layer, which can prevent the inherent optical absorption of Bi_2WO_6 and result in the rapid decrease of the quantity of photogenerated charges, and finally reduce the photoactivity (sample C500-4, with 0.2 g glucose used).

4 Conclusions

In summary, we have synthesized C–Bi_2WO_6 nanostructures by a two-step method involving a hydrothermal process in the presence of glucose and a subsequent calcination in Ar gas. The carbon existing on the surface of Bi_2WO_6 nanoparticles is free and does not affect the crystal structure and band gap of Bi_2WO_6 photocatalyst. However, it can improve the specific surface area and dye adsorption of the photocatalyst, and facilitate the transport of photogenerated electrons to dye, leading to significant improvement in the photocatalytic performance. The C–Bi_2WO_6 photocatalyst obtained with 0.04 g glucose can totally decompose RhB after 4 h irradiation under visible light. Nevertheless, the photoactivity of C–Bi_2WO_6 would be reduced if excess glucose is used during the synthesis, since thick carbon coating can prevent the inherent optical absorption of Bi_2WO_6.

Acknowledgements

Financially supported by the National Natural Science Foundation of China (No. 50872039 and 20803055), China Postdoctoral Science Foundation (20090460996) and self-determined research funds of CCNU from the colleges' basic research and operation of MOE (No. CCNU09A01019).

References

1 D. Chen and J. H. Ye, *Adv. Funct. Mater.*, 2008, **18**, 1922.
2 X. Zhao and Y. F. Zhu, *Environ. Sci. Technol.*, 2006, **40**, 3367.
3 S. Sun, W. Wang, H. Xu, L. Zhou, M. Shang and L. Zhang, *J. Phys. Chem. C*, 2008, **112**, 17835.
4 G. S. Li, D. Q. Zhang and J. C. Yu, *Chem. Mater.*, 2008, **20**, 3983.
5 H. Xue, Z. H. Li, Z. X. Ding, L. Wu, X. X. Wang and X. Z. Fu, *Cryst. Growth Des.*, 2008, **8**, 4511.
6 J. Tang, Z. Zou and J. Ye, *Angew. Chem., Int. Ed.*, 2004, **43**, 4463.
7 L. Z. Zhang, I. Djerdj, M. H. Cao, M. Antonietti and M. Niederberger, *Adv. Mater.*, 2007, **19**, 2083.
8 J. W. Tang, Z. G. Zou and J. H. Ye, *J. Phys. Chem. C*, 2007, **111**, 12779.
9 F. Gao, X. Y. Chen, K. B. Yin, S. Dong, Z. F. Ren, F. Yuan, T. Yu, Z. G. Zou and J. M. Liu, *Adv. Mater.*, 2007, **19**, 2889.
10 P. H. Borse, U. A. Joshi, S. M. Ji, J. S. Jang and J. S. Lee, *Appl. Phys. Lett.*, 2007, **90**, 034103.
11 M. Takeuchi, H. Yamashita, M. Matsuoka, T. Hirao, N. Itoh, N. Iwamoto and M. Anpo, *Catal. Lett.*, 2000, **67**, 135.
12 M. Anpo and M. Takeuchi, *J. Catal.*, 2003, **216**, 505.
13 H. Yamashita, M. Harada, J. Misaka, M. Takeuchi, B. Neppolian and M. Anpo, *Catal. Today*, 2003, **84**, 191.
14 R. Asahi, T. Morikawa, T. Ohwaki, K. Aoki and Y. Taga, *Science*, 2001, **293**, 269.
15 U. M. Shahed, A. Mofareh and B. William, *Science*, 2002, **297**, 2243.
16 S. Sakthivel and H. Kisch, *Angew. Chem., Int. Ed.*, 2003, **42**, 4908.
17 J. C. Yu, J. G. Yu, W. K. Ho, Z. T. Jiang and L. Z. Zhang, *Chem. Mater.*, 2002, **14**, 3808.
18 P. V. Kamat, *Pure Appl. Chem.*, 2002, **74**, 1693.
19 K. Awazu, M. Fujimaki, C. Rockstuhl, J. Tominaga, H. Murakam, Y. Ohki, N. Yoshida and T. Watanabe, *J. Am. Chem. Soc.*, 2008, **130**, 1676.
20 A. Furube, L. Du, K. Hara, R. Katoh and M. Tachiya, *J. Am. Chem. Soc.*, 2007, **129**, 14852.
21 P. D. Cozzoli, R. Comparelli, E. Fanizza, M. L. Curri, A. Agostiano and D. Laub, *J. Am. Chem. Soc.*, 2004, **126**, 3868.
22 B. M. Reddy, P. M. Sreekanth, E. P. Reddy, Y. Yamada, Q. A. Xu, H. Sakurai and T. Kobayashi, *J. Phys. Chem. B*, 2002, **106**, 5695.
23 H. B. Zeng, W. P. Cai, P. S. Liu, X. X. Xu, H. J. Zhou, C. Klingshirn and H. Kalt, *ACS Nano*, 2008, **2**, 1661.
24 X. P. Lin, T. Huang, F. Q. Huang, W. D. Wang and J. L. Shi, *J. Mater. Chem.*, 2007, **17**, 2145.
25 H. B. Lu, H. Li, L. Liao, J. C. Li, Y. Tian, M. Shuai, M. F. Hu and B. P. Zhu, *Nanotechnology*, 2008, **19**, 045605.
26 G. Burgeth and H. Kisch, *Coord. Chem. Rev.*, 2002, **230**, 40.
27 M. Jakob, H. Levanon and P. V. Kamat, *Nano Lett.*, 2003, **3**, 353.
28 S. H. Elder, F. M. Cot, Y. Su, S. M. Heald, A. M. Tyryshkin, M. K. Bowman, Y. Gao, A. G. Joly, M. L. Balmer, A. C. Kolwaite, K. A. Magrini and D. M. Blake, *J. Am. Chem. Soc.*, 2000, **122**, 5138.
29 S. K. Poznyak, D. Talapin and A. Kulak, *J. Phys. Chem. B*, 2001, **105**, 4816.
30 N. H. Zhao, G. J. Wang, Y. Huang, B. Wang, B. D. Yao and Y. P. Wu, *Chem. Mater.*, 2008, **20**, 2612.
31 S. Goldstein, D. Behar and J. Rabani, *J. Phys. Chem. C*, 2009, **113**, 12489.
32 S. Shanmugam, A. Gabashvili, D. S. Jacob, J. C. Yu and A. Gedanken, *Chem. Mater.*, 2006, **18**, 2275.
33 L. W. Zhang, H. B. Fu and Y. F. Zhu, *Adv. Funct. Mater.*, 2008, **18**, 2180.
34 M. Inagaki, Y. Hirose, T. Matsunaga, T. Tsumura and M. Toyoda, *Carbon*, 2003, **41**, 2619.

35 L. W. Zhang, H. Y. Cheng, R. L. Zong and Y. F. Zhu, *J. Phys. Chem. C*, 2009, **113**, 2368.
36 N. Sobana, M. Muruganandam and M. Swantinathan, *Catal. Commun.*, 2008, **9**, 262.
37 N. Sobana and M. Swantinathan, *Sol. Energy Mater. Sol. Cells*, 2007, **91**, 727.
38 A. Kudo and S. Hijii, *Chem. Lett.*, 1999, 1103.
39 J. W. Tang, Z. G. Zou and J. H. Ye, *Catal. Lett.*, 2004, **92**, 53.
40 J. G. Yu, J. F. Xiong, B. Cheng, Y. Yu and J. B. Wang, *J. Solid State Chem.*, 2005, **178**, 1968.
41 S. C. Zhang, C. Zhang, Y. Man and Y. F. Zhu, *J. Solid State Chem.*, 2006, **179**, 62.
42 C. Zhang and Y. F. Zhu, *Chem. Mater.*, 2005, **17**, 3537.
43 H. B. Fu, C. S. Pan, W. Q. Yao and Y. F. Zhu, *J. Phys. Chem. B*, 2005, **109**, 22432.
44 Y. Ebina, T. Sasaki, M. Haradav and M. Waranabe, *Chem. Mater.*, 2002, **14**, 4390.
45 L. S. Zhang, W. Z. Wang, Z. G. Chen, L. Zhou, H. L. Xu and W. Zhu, *J. Mater. Chem.*, 2007, **17**, 2526.
46 J. Wu, F. Duan, Y. Zheng and Y. Xie, *J. Phys. Chem. C*, 2007, **111**, 12866.
47 Y. Y. Li, J. P. Liu, X. T. Huang and G. Y. Li, *Cryst. Growth Des.*, 2007, **7**, 1350.
48 Y. Y. Li, J. P. Liu and X. T. Huang, *Nanoscale Res. Lett.*, 2008, **3**, 365.
49 Q. Xiao, J. Zhang, C. Xiao and X. K. Tan, *Catal. Commun.*, 2008, **9**, 1247.
50 S. B. Zhu, T. G. Xu, H. B. Fu, J. C. Zhao and Y. F. Zhu, *Environ. Sci. Technol.*, 2007, **41**, 6234.
51 L. S. Zhang, K. H. Wong, Z. G. Chen, J. C. Yu, J. C. Zhao, C. Hu, C. Y. Chan and P. K. Wong, *Appl. Catal., A*, 2009, **363**, 221.
52 Q. Peng, Y. J. Dong and Y. D. Li, *Angew. Chem.*, 2003, **115**, 3135.
53 Q. Peng, Y. J. Dong and Y. D. Li, *Angew. Chem., Int. Ed.*, 2003, **42**, 3027.
54 T. Sakaki, M. Shibata, T. Miki, H. Hirosue and N. Hayashi, *Bioresour. Technol.*, 1996, **58**, 197.
55 M. Crane, R. Frost, P. Williams and T. Kloprogge, *J. Raman Spectrosc.*, 2002, **33**, 62.